AIAA JOURNAL
Vol. 46, No. 12, December 2008

Characterization of Discharge Modes of Plasma Actuators

Dmitri M. Orlov,* Gabriel I. Font,† and Daniel Edelstein‡
U.S. Air Force Academy, Colorado Springs, Colorado 80918

DOI: 10.2514/1.37514

Atmospheric-pressure dielectric barrier discharges for aerodynamic flow control are investigated. The properties of the plasma discharge during positive and negative half-cycles of the driving voltage are studied experimentally and numerically. The simulations are performed in nitrogen. It is shown that during the positive half-cycle the plasma operates in the streamer mode, whereas the negative half-cycle is characterized by a glow-type discharge. The computational results are compared with experimental optical measurements and found to be in good agreement.

I. Introduction

PLASMA actuators are devices that can be used for flow control by promoting boundary-layer attachment over wings. If optimized, they hold the promise of reducing cruise drag and the associated fuel penalties. Plasma actuators have been previously used in different flow control applications such as leading-edge separation control on airfoils [1], drag reduction [2], bluff-body control [3–5], turbine tip-clearance flow control [6,7], low-pressure turbine-blade separation control [8,9], and excitation of instabilities on a sharp cone in supersonic flow [10]. Recent reviews on the plasma-enhanced aerodynamics by Moreau [11] and Corke et al. [12] discuss concepts, optimization, and applications of the plasma actuators.

The plasma actuator is a single dielectric barrier discharge (SDBD) device [13–16]. It consists of two electrodes arranged highly asymmetrically, as shown in Fig. 1. Typically, the electrodes are long and thin and placed spanwise on the aerodynamic surface. The electrodes are separated by the dielectric layer. One of the electrodes is exposed to the air, whereas the other electrode is covered by dielectric. In typical operation, ac voltage with high amplitude (1–20 kV) and high ac frequency (1–20 kHz) are applied to the electrodes. High electric fields cause air ionization above the dielectric surface, resulting in a body force that acts on the neutral air. The most important feature of the SDBD is that it can sustain plasma discharge at atmospheric pressure without the discharge collapsing into a constricted arc.

Extensive experimental and theoretical studies of the SDBD plasma actuators were done in recent years to understand the physics of the discharge and the body-force production mechanisms. Different experimental methods that were used include electric current and light-intensity observations [14,15,17], smoke visualization [18,19], hot wire, pitot tube, and digital particle image velocimetry measurements of plasma-induced flow velocities [18,20,21] and acoustic [22] and accelerometer measurements [23]. Recent experimental work by Enloe et al. [24] used a V-dot probe method to find the charge density on the dielectric surface inside the plasma region. The results of these studies have already led to some important optimizations of the plasma-actuator operation.

Models have also been created that allow one to incorporate plasma actuators into numerical flow solvers. These models include the spatial-temporal lumped-element circuit model by Orlov [25] and potential flow model by Hall et al. [26]. These models provide quick and efficient estimation of the plasma actuator's effects and have been successfully used in flow control applications [1,25].

Over the past years, simulations have been carried out on plasma actuators in an effort to understand the physics of the plasma formation and the interaction of the plasma with the airflow around them. These simulations include the modeling of streamer propagation in air [27,28], glow modeling using plasma fluid codes [29,30], and particle-in-cell direct simulation Monte Carlo [31,32]. Some of these simulations were successful in modeling the plasma formation or the interaction of the plasma with the air.

The purpose of the present work is to extend our understanding of the single dielectric barrier discharge in the aerodynamic plasma actuator through the detailed study of the plasma formation. Specifically, recent experiments have shown the plasma discharge changing in character during different parts of the ac bias cycle. This work carries out simulations in an effort to understand the nature of the plasma character change and the physical reasons for it. This knowledge of the plasma discharge behavior will, it is hoped, allow us to further optimize the plasma actuator for different flow control applications.

II. Problem Setup

Computations were performed using KINEMA Plasmator™ software. This software has been used previously to model different types of plasmas including glow discharges and streamers [33–36]. It has also been used to study single dielectric barrier discharge plasma actuators at atmospheric pressure [32]. The code uses a fluid approximation for the treatment of ions and electrons. It solves the continuity and energy equations for the electrons and the continuity and momentum equations for the ions. The neutrals are treated as a background gas and do not enter the simulations except as a source of chemical species and collisional momentum loss. Poisson's equation is solved self-consistently for the potential distribution.

The plasma actuator was modeled in a rectangular 2-D domain, as shown in Fig. 2. Although the plasma discharge is inherently a 3-D phenomena, this 2-D approximation allows the study of some of the discharge characteristics without incurring the additional computational cost. As will be shown subsequently, the ionization-wave and streamer-head characteristics of the real discharge are still captured. The domain dimensions were 10 by 7.5 mm. The actuator was located in the lower part of the domain, with the exposed electrode flush-mounted with the dielectric surface. The exposed electrode was 2 mm long, and the encapsulated electrode had a length of 4 mm; both electrodes were 0.2 mm thick, separated by 0.2 mm of dielectric with a dielectric coefficient of 3.5. The upper part of the domain was represented by pure nitrogen.

The boundary conditions of the simulation were as follows: the plasma potential gradient on the boundary was enforced as zero in the direction normal to the boundaries. All ions and electrons reaching the exposed electrode were neutralized. All ions impacting the dielectric or exposed electrode were candidates for secondary

Presented as Paper 1409 at the 46th AIAA Aerospace Sciences Meeting and Exhibit, Reno, NV, 7–10 January 2008; received 12 March 2008; accepted for publication 15 July 2008.

*Research Associate, Department of Physics. Member AIAA.
†Professor, Department of Physics. Member AIAA.
‡2nd Lt., Laughlin Air Force Base, TX 78843.

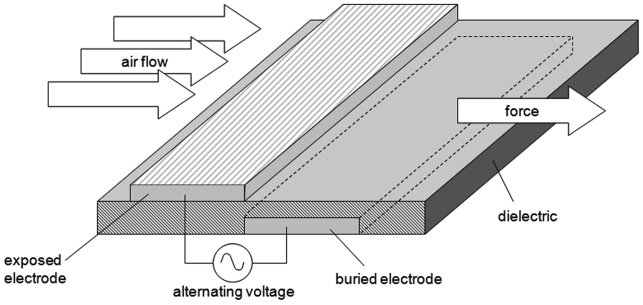

Fig. 1 Plasma-actuator configuration.

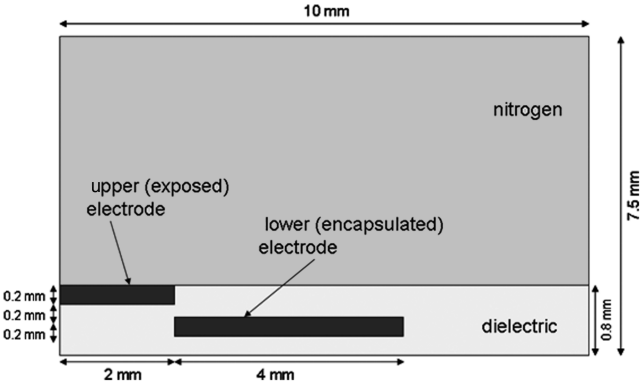

Fig. 2 Computational domain.

electron emission. The emission probability was set at 5%. This is a number that is typical of materials used in actuator construction.

The encapsulated electrode was grounded throughout the simulation with its electric potential set at 0 V. The voltage applied to the upper exposed electrode had a sinusoidal form:

$$V = -V_{\max} \sin(\omega t) \tag{1}$$

where $V_{\max}$ is the magnitude of the applied voltage, and ω is the applied ac angular frequency. To simulate linearly increasing applied voltage, we chose $V_{\max} = 50$ kV and $\omega = 2000$ rad/s. This produced a sinusoid with a large quasi-linear voltage increase rate at the beginning and middle of the ac cycle.

The real actuator will undergo thousands of cycles during operation. Charge builds up on the dielectric and directly affects the following ac cycles. Multiple ac cycles have not been modeled in the present work due to computational cost. Therefore, the effects on the discharge of charge buildup is not included. The effects will be the subject of future studies.

As it has been shown previously by Enloe et al. [37], the oxygen content greatly affects the plasma body-force production, but it only mildly changes the discharge properties. The present work does not include the effects of oxygen and the negative ions and is limited to a pure nitrogen discharge. For this reason, the forces will not be used for comparisons. Instead, the present work focuses on the plasma structure and the ability of the computations to elucidate the reasons behind the plasma structural changes noted in the experiment described subsequently. The complete list of species and chemical reactions used in the present simulation is shown in Table 1.

The computations were started with a charge density of 10^9 electrons and ions per cubic meter. This value corresponds to the observed charge density in the atmosphere under standard conditions [38]. This is a density level that provides an electron seed to the computations but does not affect the solution as determined through computational tests. The pressure was set to 1 atm.

The computations were conducted by simulating the positive and negative bias-voltage half-cycles separately. During the initial bias-voltage half-cycle, the exposed electrode is negative. This half-cycle will be termed the *forward discharge* because the electrons accelerate forward and away from the exposed electrode. The applied

Table 1 List of chemical reactions in the simulation

$e + N_2 \rightarrow N_2 + e$	Momentum transfer
$e + N_2 \rightarrow N_{2A} + e$	Excitation
$e + N_2 \rightarrow N_{2a} + e$	Excitation
$e + N_2 \rightarrow e + N + N$	Dissociation
$e + N_2 \rightarrow N_2^+ + e + e$	Ionization
$e + N_{2a} \rightarrow N_2^+ + e + e$	Ionization
$e + N_{2A} \rightarrow N_2^+ + e + e$	Ionization
$e + N_2^+ \rightarrow N + N$	Dissociative recombination
$N_{2A} \rightarrow N_2$	Deexcitation
$N_{2a} \rightarrow N_2$	De-Excitation
$N + N \rightarrow N_2$	Re-Association
$N_2^+ + \text{surface} \rightarrow N_2 + e$	Secondary electron emission

voltage was initially set at −2.2 kV and decreased throughout the computations, reaching −10 kV by the end of the simulation.

During the second bias-voltage half-cycle, the exposed electrode is positive. This half-cycle will be termed the *back discharge* because the electrons accelerate backward and toward the exposed electrode. The applied voltage was initially set at 2.2 kV and increased approximately linearly throughout the computations, reaching 15.4 kV by the end of the simulation.

In an actual discharge, the charge deposited on the dielectric by the forward discharge directly affects the back discharge. The present work, however, models the forward and backward discharges independently in an effort to isolate the plasma structural differences due to the driving voltage.

III. Results and Discussion

We used high-speed charge-coupled device camera technology to image the plasma actuator. The photographs were taken from above the actuator and the exposure time was made small enough, about 20 μs, to capture the structure of the plasma, at least within the limits of what can be discerned from visible light. Phase-locking the exposures to the voltage driving signal allowed the forward and back discharges to be imaged separately. During both the forward and back discharges, the plasma begins at the exposed electrode and expands away from it. The results of the experimental photographs were quite striking. Figure 3 shows two images that are representative of the hundreds of images taken.

The forward discharge, when the exposed electrode is negative, appears as a diffuse glow emanating from discrete locations on the exposed electrode. The photographs suggest that the plasma microdischarges begin at discrete locations. Comparisons of multiple photographs indicate that these initiation points change location between different ac cycles. They may, in fact, change

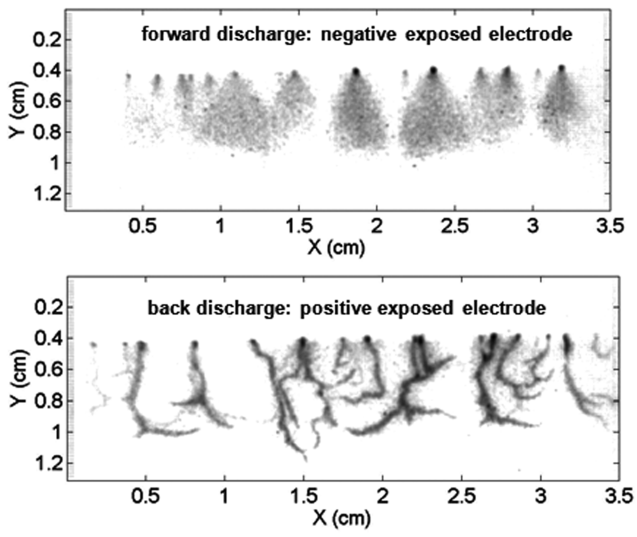

Fig. 3 Experimental overhead short exposure photos of plasma-actuator discharge.

location during a single cycle, but that has not yet been experimentally determined. Each microdischarge lasts several microseconds. The back discharge, when the exposed electrode is positive, appears very different. It is composed of thin discrete filaments that propagate from specific locations on the exposed electrode. Again, the locations at which the filaments start are not constant between bias cycles. The filaments themselves, like the forward discharges, only exist for several microseconds. In the hundreds of photographs taken, these general features did not change. The forward discharge was always diffuse and the back discharge was always filamentary. A full analysis of these photographs is beyond the scope of this paper. However, one fact is clearly borne out by them: the forward and back discharges have remarkably different plasma structures. The forward discharge resembles a glow- or Townsend-type discharge, whereas the back discharge appears to be of a streamer type.

In an effort to clarify the nature of the discharge, computations were conducted, as described previously, of the discharge while the voltage of the exposed electrode was positive and increasing and while it was negative and becoming more negative. This was meant to roughly simulate the parts of the sinusoidal driving voltage in which plasma is experimentally observed to exist [14,15]. The resulting plasma, for both cases, was observed to grow and diminish in the computations as the microdischarges were spontaneously created and extinguished, whereas the absolute magnitude of the driving voltage increased. This is most clearly seen in the normalized total-force-vs-time plot displayed in Fig. 4 for forward and back discharges. Each microdischarge creates a large number of ions that accelerate in the electric field and impart momentum to the air. Between the microdischarges, the plasma decays and the density falls. Consequently, the force imparted also diminishes.

The repeating microdischarges do not exist in the computations unless the voltage magnitude is increasing. This is important. If the voltage is held constant, the computations capture only a single microdischarge. The frequency of the microdischarges cannot yet be correlated with experiments, probably due to the 2-D nature of the computations in contrast to the 3-D nature of the actual discharge. The forward discharge, however, appears to have a microdischarge frequency more than 4 times higher than the frequency of the back discharge. The fact that the computations capture the repeating microdischarges is, nevertheless, encouraging and lends confidence in the computations. The experimental existence of the microdischarges is supported from the experimental light and current measurements. Direct comparison with the forces, however, is not yet possible, due to our inability to experimentally measure the force generated by the discharge on the time scales of the microdischarges.

To understand the structural differences in the forward and back discharges, the details of the microdischarges themselves must be examined. Figure 5 shows the plasma net charge density $n_{\text{ion}} - n_{\text{electron}}$ during the beginning, middle, and end of one microdischarge for the forward (exposed electrode negative) and the back (exposed electrode positive) discharges. The density is reported for a location 0.1 mm above the dielectric surface. During the forward discharge, each individual microdischarge does not change its spatial relation with respect to the exposed electrode. The high-density region begins near the exposed electrode and remains near the exposed electrode until the discharge is extinguished. Conversely, during the back discharge, each microdischarge has a region of high plasma density that moves along the surface in a direction away from the exposed electrode. The areas in front and behind the high-density region have significantly lower plasma density.

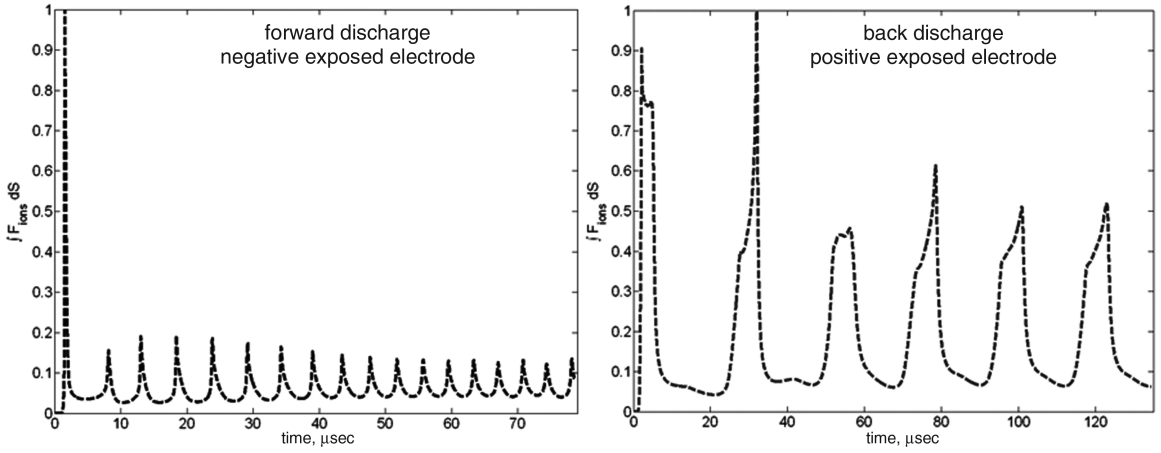

Fig. 4 Time history of normalized total force during forward and back microdischarges.

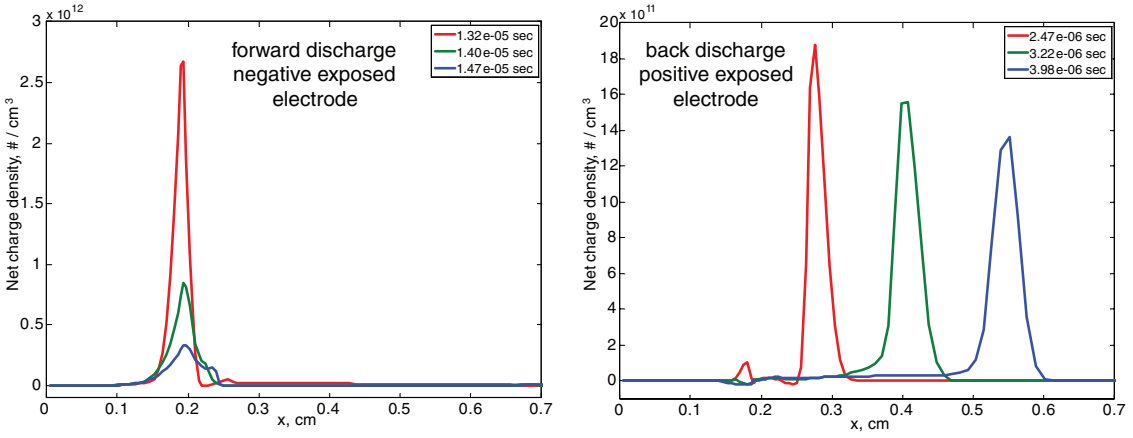

Fig. 5 Plasma net charge density during start, middle, and end of microdischarge.

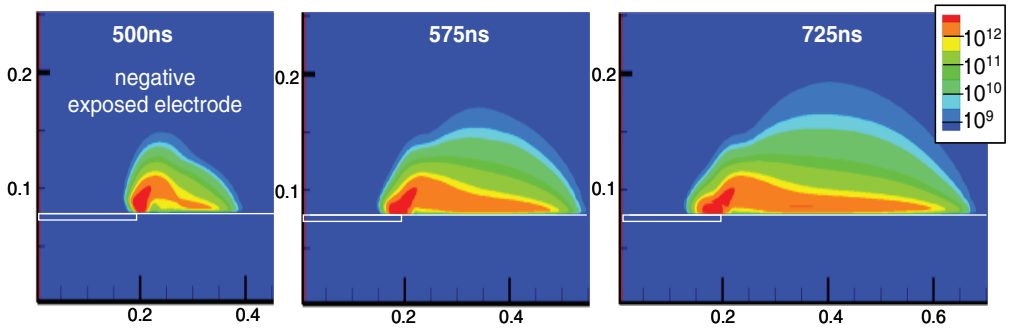

Fig. 6 Ion-density contours (cm^{-3}) during a diffuse microdischarge; dimensions are in centimeters.

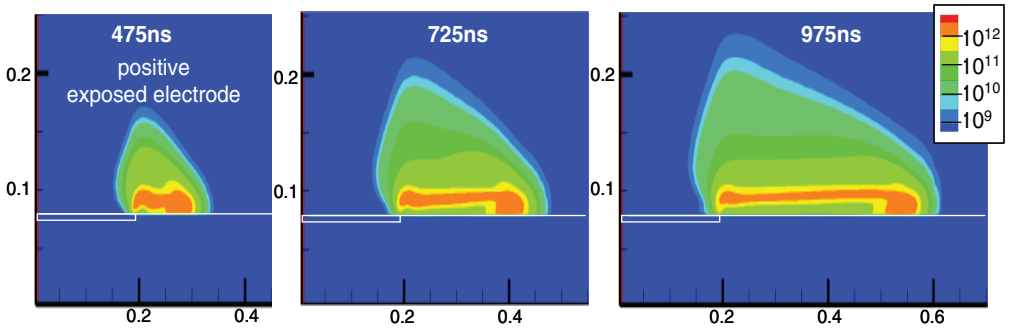

Fig. 7 Ion-density contours (cm^{-3}) during a filamentary microdischarge; dimensions are in centimeters.

This behavior is further illustrated by the spatial distribution of ion-density contours shown in Figs. 6 and 7 for both the forward and back discharges, respectively. The vertical spatial scale is exaggerated for clarity. During the forward microdischarge, the plasma is created near the exposed electrode. Its high-density region remains near the exposed electrode during the entire microdischarge. Although the plasma extends over the dielectric, the density magnitude diminishes as the distance to the exposed electrode increases. During the back discharge, a much different photograph emerges. The plasma is initially created near the exposed electrode, but its high-density region does not remain static. Instead, it travels along the dielectric as plasma grows. At the end of the back discharge, the highest-density region is located at the point farthest away from the exposed electrode.

The final clue as to the nature of the microdischarges is found in the electric field. The contours of the electric field for a forward and back microdischarge are shown in Figs. 8 and 9, respectively. During the forward discharge, the high-electric-field region, capable of causing gas breakdown, remains near the edge of the exposed electrode. Conversely, during the back discharge, the high-electric-field region travels with the high-plasma-density region along the dielectric and away from the exposed electrode.

The plots of plasma density and electric field suggest that the forward discharge is of a glow type. The high-electric-field region (greater than 30 kV/cm) causes the gas to breakdown. The liberated electrons are accelerated by the electric field and cause further ionization. The plasma does not intensify as it moves away from the exposed electrode, because the electrons are moving out of the high-electric-field region and consequently find it increasingly difficult to gain enough energy between collisions to cause further ionization. Therefore, the computations confirm what the experimental photographs suggested: the forward discharge is similar to a Townsend- or glow-type discharge mode.

The back discharge appears to be very different. The region in which the electric field is sufficiently large to cause gas breakdown moves with the leading edge or the head of the plasma. The density remains high in this region as well as along a narrow channel leading back to where the discharge was initiated as the plasma spreads along the dielectric. This is characteristic of a streamer-type discharge [39], in which the electric fields in the head of the streamer are sufficiently large to cause the continual ionization and self-propagation of the plasma-ionization front. This again confirms what was suggested by the experimental photographs: the back discharge is of a streamer-type plasma mode.

A logical question now arises as to why a negative decreasing voltage causes a glow plasma for essentially symmetric external driving voltage conditions, whereas a positive increasing voltage of the same magnitude and rate of increase causes a streamer-type plasma. In other words, a symmetric driving voltage produces an asymmetric discharge. Both should have the same electric field

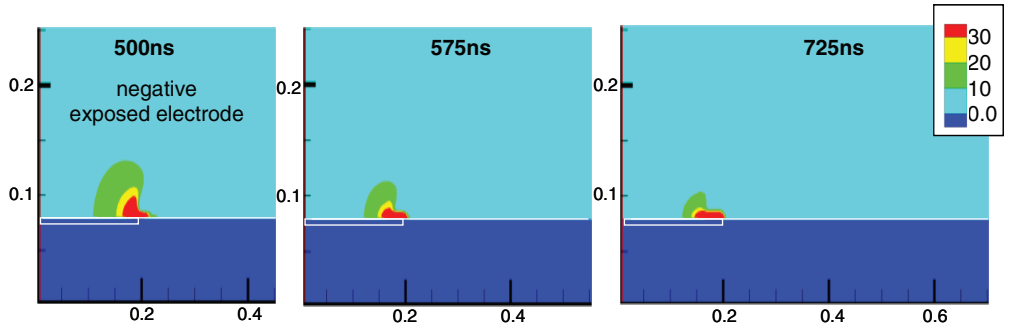

Fig. 8 Electric field magnitude contours (kV/cm) during a diffuse microdischarge; dimensions are in centimeters.

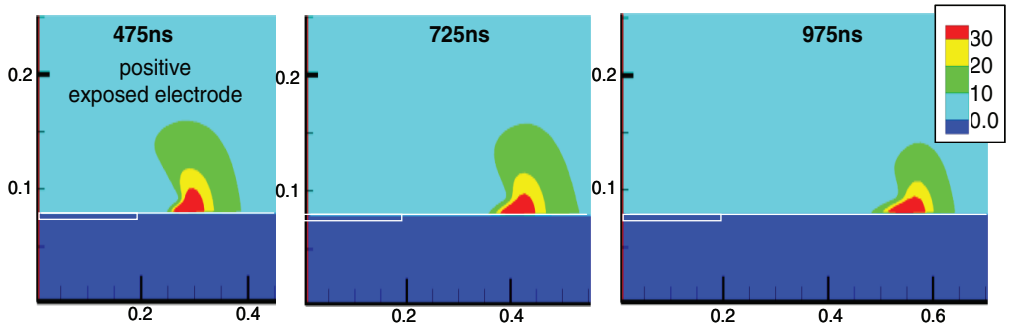

Fig. 9 Electric field magnitude contours (kV/cm) during a filamentary microdischarge; dimensions are in centimeters.

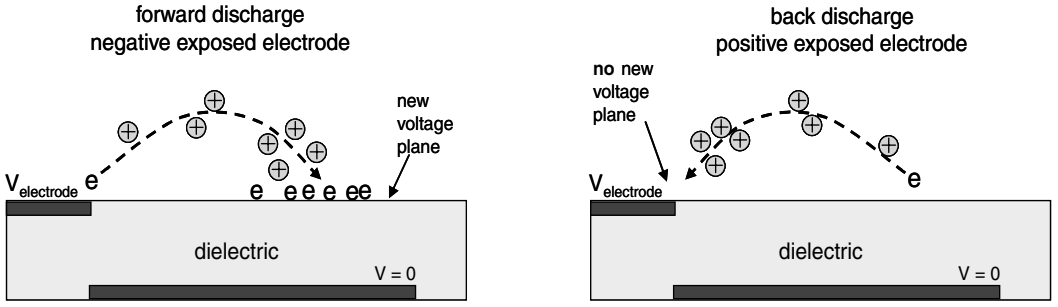

Fig. 10 Schematic of how electrons landing on the dielectric during the forward discharge create a new voltage plane and shield out the electric field. During the back discharge, the electrons enter the exposed electrode and no new voltage plane is created.

magnitude and rate of electric field increase. The answer is suggested by the schematic presented in Fig. 10. When the exposed electrode is negative,

1) The electrons accelerate in a direction away from the electrode.
2) The electrons cause further ionization.
3) The electrons land and remain on the dielectric.

In the time scale of the microdischarges, the ions do not move any significant distance, due to the high number of collisions that they undergo with the atmospheric-pressure neutral gas. The large amount of electrons that land on the surface then shield out the electric field by creating a second voltage plane at the dielectric surface. The electric field therefore never rises to a point at which a streamer discharge is initiated.

Conversely, when the exposed electrode is positive,

1) The electrons accelerate toward the electrode.
2) The electrons cause further ionization.
3) The electrons land on the exposed electrode and are absorbed into the conduction bands of the metal.

In this case, no new voltage plane is created and no shielding takes place. The voltage difference between the exposed electrode and the dielectric is therefore allowed to rise to a point at which a streamer discharge is initiated.

This postulation is confirmed by Fig. 11, which displays the voltage difference between the exposed electrode and the dielectric surface during multiple forward and back microdischarges. During the forward discharge, the average voltage difference is only about 200 V. The exposed electrode potential itself continues to increase to thousands of volts. Because of the small repetitive discharges, however, the difference between the dielectric and the electrode remains less than several hundred volts. During the back discharge, a very different situation arises. Because the electrons cannot shield out the electric field by creating a new voltage plane at the exposed electrode, the voltage difference rises to more than 1000 V and a streamer discharge is initiated. The voltage difference does not continue to increase, because the streamer deposits a small amount of positive charge on the dielectric, which begins to shield out the

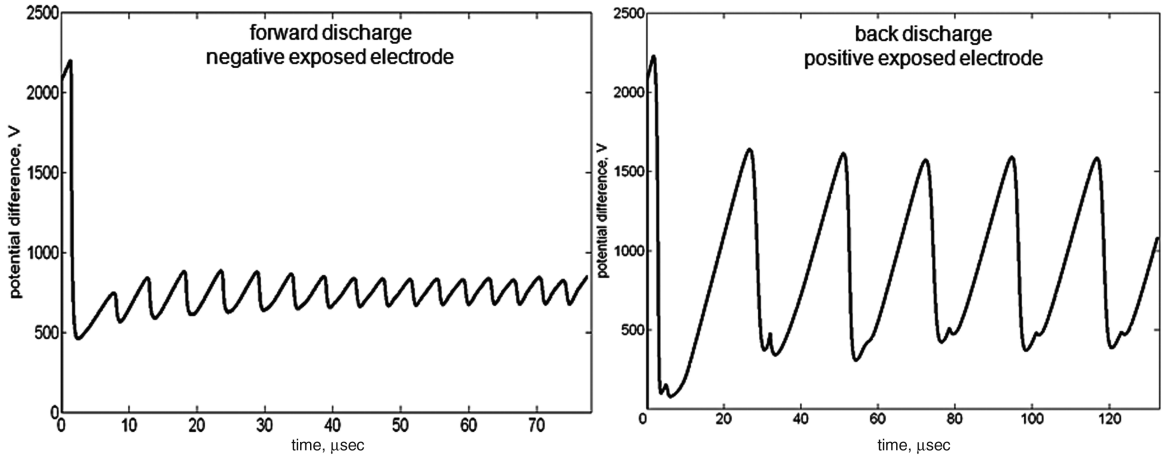

Fig. 11 Time history of the difference between the exposed electrode voltage and the average dielectric surface voltage.

electric field. The positive charge deposited at the dielectric during the back discharge is less than during the forward discharge, because the ions are many orders of magnitude less mobile than the electrons. Therefore, less ions can reach the dielectric in the same amount of time. It must be understood that this is a dynamic situation related to the rate of voltage increase (ac frequency). If sufficient time was allowed (tens of microseconds), all of the ion charge would also be able to reach the dielectric.

IV. Conclusions

Differences have been observed in the plasma structure, as shown by experimental short-exposure photographs taken during positive and negative bias half-cycles of a plasma actuator. During the negative half-cycle, the plasma is diffuse and resembles a glow discharge. During the positive half-cycle, the plasma resembles a streamer discharge. Simulations were conducted of the forward and back discharges with a fluid plasma code in an effort to explain this behavior. The plasma code was able to reproduce the experimentally observed repeating microdischarges and alternating plasma discharge modes. During the negative half-cycle, the computations exhibited a glow-type discharge, whereas during the positive half-cycle, the computations showed a streamer-type discharge. Simulations suggest that the difference in discharge mode is primarily governed by the buildup of charge on the dielectric above the encapsulated electrode. During the forward discharge, electrons created by the plasma discharge land on the dielectric and create a new voltage plane that shields out the majority of the external electric field. This keeps the local electric fields from growing sufficiently large to cause streamer formation. During the back discharge, the exposed electrode absorbs the arriving electrons and no new voltage plane is created. The result is that the electric field during the back discharge grows, due to a lack of shielding, until a streamer breakdown is initiated.

Acknowledgments

The authors gratefully acknowledge Keith Bergeron and the support of the U.S. Air Force Academy (USAFA) Modeling and Simulation Research Center as well as Thomas McLaughlin and the USAFA Aeronautics Research Center for supporting this research program. The authors would also like to thank Lon Enloe and Geoff McHarg for helpful discussions.

References

[1] Orlov, D., Apker, T., He, C., Othman, H., and Corke, T., "Modeling and Experiment of Leading Edge Separation Control Using SDBD Plasma Actuators," AIAA Paper 2007-0877, 2007.

[2] Wilkinson, S. P., "Investigation of an Oscillating Surface Plasma for Turbulent Drag Reduction," AIAA Paper 2003-1023, 2003.

[3] Thomas, F. O., Kozlov, A., and Corke, T. C., "Plasma Actuators for Bluff Body Flow Control," AIAA Paper 2006-2845, 2006.

[4] Sung, Y., Kim, W., Mungal, M. G., and Cappeli, M., "Aerodynamic Modification of Flow over Bluff Objects by Plasma Actuation," *Experiments in Fluids*, Vol. 41, No. 3, Sept. 2006, pp. 479–486. doi:10.1007/s00348-006-0175-0

[5] Artana, G., Sosa, R., Moreau, E., and Touchard, G., "Control of the Near-Wake Flow Around a Circular Cylinder with Electrohydrodynamic Actuators," *Experiments in Fluids*, Vol. 35, No. 6, Dec. 2003, pp. 580–588. doi:10.1007/s00348-003-0704-z

[6] Douville, T., Stephens, J., Corke, T., and Morris, S., "Turbine Blade Tip Leakage Flow Control by Partial Squealer Tip and Plasma Actuators," AIAA Paper 2006-0020, 2006.

[7] Van Ness, D. K., Corke, T. C., and Morris, S. C., "Turbine Tip Clearance Flow Control Using Plasma Actuators," AIAA Paper 2006-0021, 2006.

[8] Huang, J., Corke, T. C., and Thomas, F. O., "Plasma Actuators for Separation Control of Low Pressure Turbine Blades," AIAA Paper 2003-1027, 2003.

[9] List, J., Byerley, A. R., McLaughlin, T. E., and Van Dyken, R. D., "Using a Plasma Actuator to Control Laminar Separation on a Linear Cascade Turbine Blade," AIAA Paper 2003-1026, 2006.

[10] Matlis, E. H., "Controlled Experiments on Instabilities and Transition to Turbulence on a Sharp Cone at Mach 3.5," Ph.D. Dissertation, Univ. of Notre Dame, Notre Dame, IN, 2004.

[11] Moreau, E., "Airflow Control by Non-Thermal Plasma Actuators," *Journal of Physics D: Applied Physics*, Vol. 40, No. 3, 2007, pp. 605–636. doi:10.1088/0022-3727/40/3/S01

[12] Corke, T., Post, M., and Orlov, D., "SDBD Plasma Enhanced Aerodynamics: Concepts, Optimization, and Applications," *Progress in Aerospace Sciences*, Vol. 43, Nos. 7–8, Oct.–Nov. 2007, pp. 193–217. doi:10.1016/j.paerosci.2007.06.001

[13] Corke, T., Jumper, E., Post, M., Orlov, D., and McLaughlin, T., "Application of Weakly-Ionized Plasmas as Wing Flow-Control Devices," AIAA Paper 2002-0350, 2002.

[14] Enloe, C. L., McLaughlin, T. E., Van Dyken, R. D., Kachner, K. D., Jumper, E. J., and Corke, T. C., "Mechanisms and Responses of a Single-Dielectric Barrier Plasma Actuator: Plasma Morphology," *AIAA Journal*, Vol. 42, No. 3, 2004, pp. 589–594. doi:10.2514/1.2305

[15] Enloe, C. L., McLaughlin, T. E., Van Dyken, R. D., Kachner, K. D., Jumper, E. J., and Corke, T. C., "Mechanisms and Responses of a Single-Dielectric Barrier Plasma Actuator: Geometric Effects," *AIAA Journal*, Vol. 42, No. 3, 2004, pp. 595–604. doi:10.2514/1.3884

[16] Post, M., and Corke, T., "Separation Control on High Angle of Attack Airfoil Using Plasma Actuators," *AIAA Journal*, Vol. 42, No. 11, 2004, pp. 2177–2184. doi:10.2514/1.2929

[17] Enloe, C., McLaughlin, T., Van Dyken, R., and Fuscher, J., "Plasma Structure in the Aerodynamic Plasma Actuator," AIAA Paper 2004-0844, 2004.

[18] Post, M. L., "Phased Plasma Actuators for Unsteady Flow Control," M.S. Thesis, Univ. of Notre Dame, Notre Dame, IN, 2001.

[19] Roth, J., Sherman, D., and Wilkinson, S., "Electrohydrodynamic Flow Control with a Glow-Discharge Surface Plasma," *AIAA Journal*, Vol. 38, No. 7, 2000, pp. 1166–1172. doi:10.2514/2.1110

[20] Post, M. L., "Plasma Actuators for Separation Control on Stationary and Unstationary Airfoils," Ph.D. Dissertation, Univ. of Notre Dame, Notre Dame, IN, 2004.

[21] Forte, M., Jolibois, J., Moreau, E., Touchard, G., and Cazalens, M., "Optimization of a Dielectric Barrier Discharge Actuator by Stationary and Instationary Measurements of the Induced Flow Velocity, Application to Airflow Control," AIAA Paper 2006-2863, 2006.

[22] Baird, C., Enloe, C., McLaughlin, T., and Baughn, J., "Acoustic Testing of the Dielectric Barrier Discharge (DBD) Plasma Actuator," AIAA Paper 2005-0565, 2005.

[23] Porter, C., Baughn, J., McLaughlin, T., Enloe, C., and Font, G., "Temporal Force Measurements on an Aerodynamic Plasma Actuator," AIAA Paper 2006-104, 2006.

[24] Enloe, C. L., Font, G. I., McLaughlin, T. E., and Orlov, D., "Surface Potential and Longitudinal Electric Field Measurements in the Aerodynamic Plasma Actuator," *AIAA Journal* (to be published).

[25] Orlov, D., "Modelling and Simulation of Single Dielectric Barrier Discharge Plasma Actuators," Ph.D. Dissertation, Univ. of Notre Dame, Notre Dame, IN, 2006.

[26] Hall, K., Jumper, E. J., Corke, T. C., and McLaughlin, T. E., "Potential Flow Model of a Plasma Actuator as a Lift Enhancement Device," AIAA Paper 2005-0783, 2005.

[27] Likhanskii, A. V., Shneider, M. N., Macheret, S. O., and Miles, R. B., "Modeling of Interaction Between Weakly Ionized Near-Surface Plasmas and Gas Flow," AIAA Paper 2006-1204, 2006.

[28] Boeuf, J. P., Lagmich, Y., Callegari, Th., and Pitchford, L. C., "EHD Force in Dielectric Barrier Discharges Parametric Study and Influence of Negative Ions," AIAA Paper 2007-0183, 2007.

[29] Roy, S., and Gaitonde, D. V., "Modeling Surface Discharge Effects of Atmospheric RF on Gas Flow Control," AIAA Paper 2005-0160, 2005.

[30] Roy, S., Pandey, B., Poggie, J., and Gaitonde, D. V., "Modeling Low Pressure Collisional Plasma Sheath with Space-Charge Effect," *Physics of Plasmas*, Vol. 10, No. 6, 2003, pp. 2578–2585. doi:10.1063/1.1572491

[31] Font, G., "Boundary Layer Control with Atmospheric Plasma Discharges," AIAA Paper 2004-3574, 2004.

[32] Font, G. I., Enloe, C. L., McLaughlin, T. E., and Orlov, D., "Plasma Discharge Characteristics and Experimentally Determined Boundary Conditions for a Plasma Actuator," AIAA Paper 2007-0188, 2007.

[33] Stewart, R. A., Vitello, P., and Graves, D. B., "Two-Dimensional Fluid Model of High Density Inductively Coupled Plasma Sources," *Journal*

of Vacuum Science and Technology B (Microelectronics and Nanometer Structures), Vol. 12, No. 1, 1994, pp. 478–485. doi:10.1116/1.587102.

[34] Bukowski, J. D., Graves, D. B., and Vitello, P., "Two-Dimensional Fluid Model of an Inductively Coupled Plasma with Comparison to Experimental Spatial Profiles," *Journal of Applied Physics*, Vol. 80, No. 5, Sept. 1996, pp. 2614–2623. doi:10.1063/1.363169

[35] Jaeger, E. F., Berry, L. A., Tolliver, J. S., and Batchelor, D. B., "Power Deposition in High-Density Inductively Coupled Plasma Tools for Semiconductor Processing," *Physics of Plasmas*, Vol. 2, No. 6, 1995, pp. 2597–2604. doi:10.1063/1.871222

[36] Vitello, P. A., Penetrante, B. M., and Bardsley, J. N., "Simulation of Negative-Streamer Dynamics in Nitrogen," *Physical Review E (Statistical Physics, Plasmas, Fluids, and Related Interdisciplinary Topics)*, Vol. 49, No. 6, 1994, pp. 5574–5598. doi:10.1103/PhysRevE.49.5574

[37] Enloe, C. L., McLaughlin, T. E., Font, G. I., and Baughn, W., "Parameterization of Temporal Structure in the Single Dielectric Barrier Aerodynamic Plasma Actuator," AIAA Paper 2005-0564, 2005.

[38] Jursa, A. S., *Handbook of Geophysics and the Space Environment*, U.S. Air Force Geophysics Lab., Springfield, VA, 1985.

[39] Bazelyan, E. M., and Raizer, Y. P., *Spark Discharge*, CRC Press, Boca Raton, FL, 1998.

A. Tumin
Associate Editor